ADVANCED MATERIALS

Supporting Information

for *Adv. Mater.*, DOI 10.1002/adma.202303226

Monodispersed Sub-1 nm Inorganic Cluster Chains in Polymers for Solid Electrolytes with Enhanced Li-Ion Transport

Yu Cheng, Xiaowei Liu, Yaqing Guo, Guangyao Dong, Xinkuan Hu, Hong Zhang, Xidan Xiao, Qin Liu, Lin Xu and Liqiang Mai**

Supporting Information

Monodispersed Sub-1 nm Inorganic Cluster Chains in Polymers for Solid Electrolytes with Enhanced Li-Ion Transport

Yu Cheng, Xiaowei Liu, Yaqing Guo, Guangyao Dong, Xinkuan Hu, Hong Zhang, Xidan Xiao, Qin Liu, Lin Xu, Liqiang Mai**

Y. Cheng, X. W. Liu, G. Y. Dong, X. K. Hu, H. Zhang, X. D. Xiao, Q. Liu, Prof. L. Xu, Prof. L. Q. Mai

State Key Laboratory of Advanced Technology for Materials Synthesis and Processing, School of Materials Science and Engineering, Wuhan University of Technology, Wuhan 430070, China.

Prof. L. Xu, Prof. L. Q. Mai
Hubei Longzhong Laboratory, Wuhan University of Technology (Xiangyang Demonstration Zone), Xiangyang 441000, Hubei, China.
Hainan Institute, Wuhan University of Technology, Sanya 572000, China.

Dr. Y. Q. Guo,
State Key Laboratory of Materials Processing and Die & Mould Technology, School of Materials Science and Engineering, Huazhong University of Science and Technology, Wuhan 430074, China

E-mails: linxu@whut.edu.cn; mlq518@whut.edu.cn

Synthesis of the inorganic cluster chain material

The synthesis of the gadolinium oxyhydroxide inorganic cluster chain is as follows. 1.4 g $GdCl_3$ $6H_2O$ (99.9% metals basis, Aladdin) was dissolved in 1.8 mL deionized water, and then 21 mL ethanol was added and mixed well. 7 mL oleylamine and 3.5 mL oleic acid were added in 50 mL hydrothermal kettle and keep mixing. After stirring and mixing evenly, the mixed $GdCl_3$ $6H_2O$ solution was slowly added in the hydrothermal kettle under stirring (1 drop per second). After stirring for 15 min, the hydrothermal kettle was sealed and placed at 160 °C oven for 8 h. After the reaction finished, the sample was washed by ethanol and DI water for 3 times and kept in cyclohexane. The synthesis of common nanowires in the control group was carried out by adjusting the proportion of oleylamine and oleic acid, and prolonging the reaction time.

Fabrication of the composite solid-state electrolyte

The as-obtained GdOOH cluster chains were washed out of cyclohexane after settling with ethanol, and the dispersed in the mixed solvent of Tetrahydrofuran (THF) and Dichloromethane (DCM) (50:50 vol), then kept ultrasonic for 2 h until the mixture is totally transparent. PEO (M_W=600000 g mol^{-1}, Sigma-Aldrich) and lithium salt (LiTFSI, Aladdin) were dissolved in another glass of mixed solvent and kept stirring for 1 h under 40 °C until the mixture became transparent, where the mole ratio of ethylene oxide [EO] to [Li] was 8:1. Next, the cluster chain transparent mixture was slowly dropped into the stirring polymer electrolyte mixture, and make sure that the composite mixture kept transparent all the time. Afterwards, the composite mixture was continuously stirred in the Batidora Planetaria (SpeedMixerTM DAC 150.1 FVZ) under a speed of 3000 rpm to promote the dispersion of cluster chain in the polymer matrix. Then, the composite electrolyte mixture was stirring for 12 h under 35 °C. After that, the composite mixture is poured into PTFE module and dried in vacuum oven of 45 °C for 6 h and then 60 °C for 12 h. Finally, the prepared composite solid-state electrolyte films needed to be placed in a glove box filled with argon for subsequent use. The electrolyte membrane with thickness of ~110 μm can be produced.

The fabrication of the composite SSE for control groups followed the same process, that was, the inorganic filler and polymer solid electrolyte were separately dispersed in the specific mixture, and then added the mixture of the inorganic filler into the polymer solid electrolyte mixture while stirring. The SSE preparation processes should be carried out in an Ar-filled glovebox with H_2O and O_2 contents below 0.1 ppm to isolate water and oxygen.

Fabrication of the composite cathode and cell assembly

The $LiFePO_4$ (1 C=170 mAh g^{-1}) and $LiNi_{0.8}Co_{0.1}Mn_{0.1}O_2$ (NCM811) (1 C = 180 mAh g^{-1}) composite cathode were fabricated by the same facile coating method. The active cathode powder, conductive additives (Super P), composite SSE (15 mg mL^{-1}, in liquid mixture), and PVDF powder (70:10:10:10 by solid weight ratio) were mixed with magnetic stirring for 6 hours. Then, the composite slurry was coated on an aluminum current collector and vacuum dried at 45 °C for 6 h and then 60 °C for 12 h. All the preparation processes should be carried out in an Ar-filled glovebox with H_2O and O_2 contents below 0.1 ppm. The active cathode material loading for the coin cells and pouch cells was ~2 mg cm^{-2}. No liquid additive was added during the cell assembling process.

Materials Characterizations

X-ray diffraction (XRD) patterns were recorded using a D8 discover X-ray diffractometer with Cu Kα radiation. The thermal stability was executed by thermogravimetric analysis (TGA) using a NETZSCH STA 449F5 instrument over the temperature range between 25 °C and 600 °C under Air flux at a heating rate of 10 °C min^{-1}. Differential scanning calorimetry (DSC) was conducted by TA-DSC 2500 from -80 °C to 0 °C, Scanning electron microscopy (SEM) was represented by scanning electron microscope (JEOL-7100F). Energy dispersive spectrometer (EDS) was collected by an Oxford IE250 system. Transmission electron microscopy (TEM) and scanning transmission electron microscopy (STEM) patterns were performed by Talos F200 S. X-ray photoelectron spectroscopy (XPS) analysis was performed using

a VG MultiLab 2000. Fourier transform infrared spectrometer (FT-IR) was measured via Thermo Nicolet Corporation. ^{7}Li solid-state Nuclear Magnetic Resonance (NMR) was measured by Bruker Avance Neo 400WB. TOF-SIMS measurements were conducted with a PHI nano TOF III. A Bi_3^{++} beam (3 kV, 2 nA) with raster size of 100um was used as the primary beam to detect the samples, sputtering with an Ar^+ beam (2 kV, 100 nA, 400×400 μm^2) was applied for depth profiling analysis. The sputtering rate is ~9.16 nm/min on SiO_2. The accelerating rate calorimeter (ARC) tests of the 100 mAh NCM/Li pouch cells (100% SOC) were investigated in the HWS mode. The heating step was 5 °C, the thermal runaway criteria was 1 °C min^{-1}, and the detection limit was 0.02 °C min^{-1}.

Electrochemical Measurements:

Electrochemical impedance spectroscopy (EIS) was tested by assembling blocking stainless steel|SSEs|stainless steel (SS) cell from 10^6 to 0.1 Hz with an amplitude of 10 mV via Autolab PGSTAT302N. The electrochemical stability window was tested by linear sweep voltammetry (LSV) on a lithium|SSEs|stainless steel cell from 0 to 6.5 V via Autolab PGSTAT302N at a scan rate of 1 mV s^{-1}. The ionic conductivity (σ) was calculated according to Equation (1), which *L* is *S* as the effective contacting area among SSE and SS, *R* presents the resistance value of the bulk electrolyte, and *L* the thickness of the SSE.

$$\sigma = \frac{L}{S \cdot R} \tag{1}$$

Arrhenius plots were obtained by calculating ionic conductivity at a temperature range of 20-80 ℃ via Autolab PGSTAT302N. *A* is conductivity pre-exponential factor, *E*a is the activation energy, and *T* is the absolute temperature, *R* is the ideal gas constant. The computational formula of the activation energies (Ea): The Ea of solid electrolytes was calculated by Arrhenius relation from Equation (2)

$$\sigma(T) = A \exp\left(-\frac{Ea}{RT}\right) \tag{2}$$

The Li||Li symmetrical cells assembled with GTSSE was measured by chronoamperometry method, a polarization of 10 mV (Δ*V*) was applied to the cells for

5,000 seconds. The polarization currents of cell including initial (I_0) and steady-state (I_s) were recorded. The interfacial resistances before (R_0) and after (R_s) polarization were tested by alternating current impedance. Afterwards, t_{Li^+} was calculated from Bruce-Vincent-Evans Equation (3):

$$t_{Li^+} = \frac{I_S(\Delta V - I_0 R_0)}{I_0(\Delta V - I_S R_S)} \quad (3)$$

The cycling stability of lithium|SSEs|lithium, and SSLB was conducted using a multichannel battery testing system (LAND CT2001A). The full cells were assembled with composite cathode, SSE, and lithium metal anodes via ordinal stacking. The cycle performance of Li||LFP cell is tested between 2.7 and 4.0 V. The cycle performance of Li||NCM811 cell is tested between 2.7 and 4.3 V. All the electrochemical properties of SSLBs and lithium symmetric cells were tested at 60 °C. As for some SSLBs cycling tests of the control groups (LFP 1 C, NCM811 0.5 C), the first three cycles are activated at 0.1 C.

Theoretical calculation method

The corrected charges simulations of these molecules were conducted by a Materials Studio software, reversion 2018 within a DFT theory. Following geometry optimization and transition state search processes were both operated in CASTEP package. And a pure density functional method PBE, which is one of the most popular formulations in generalized gradient approximation (GGA) method was adapt in these simulations.

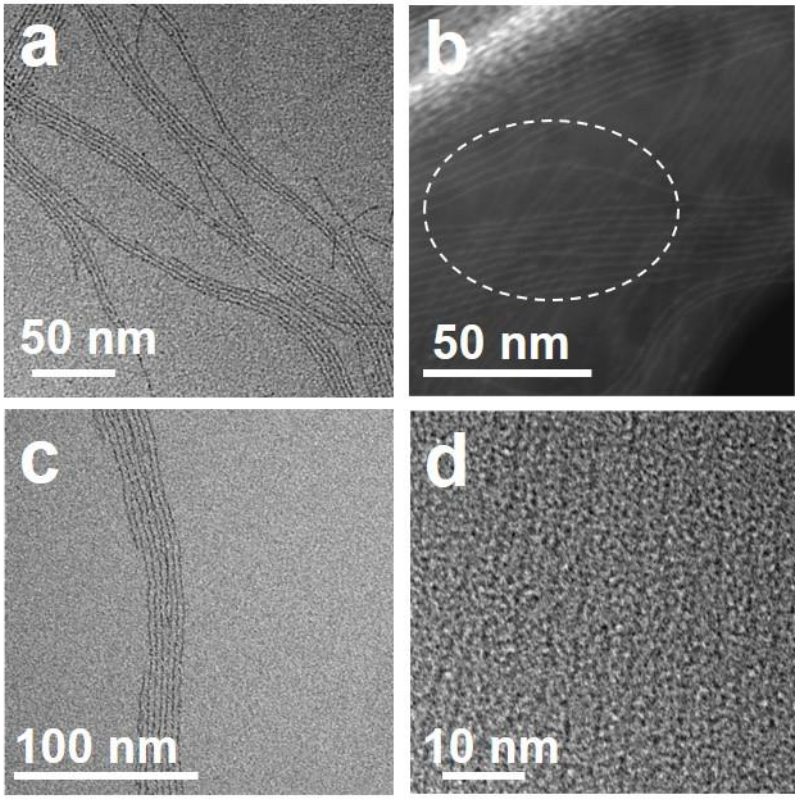

Figure S1. TEM a,c,d) and STEM b) images of inorganic cluster chains.

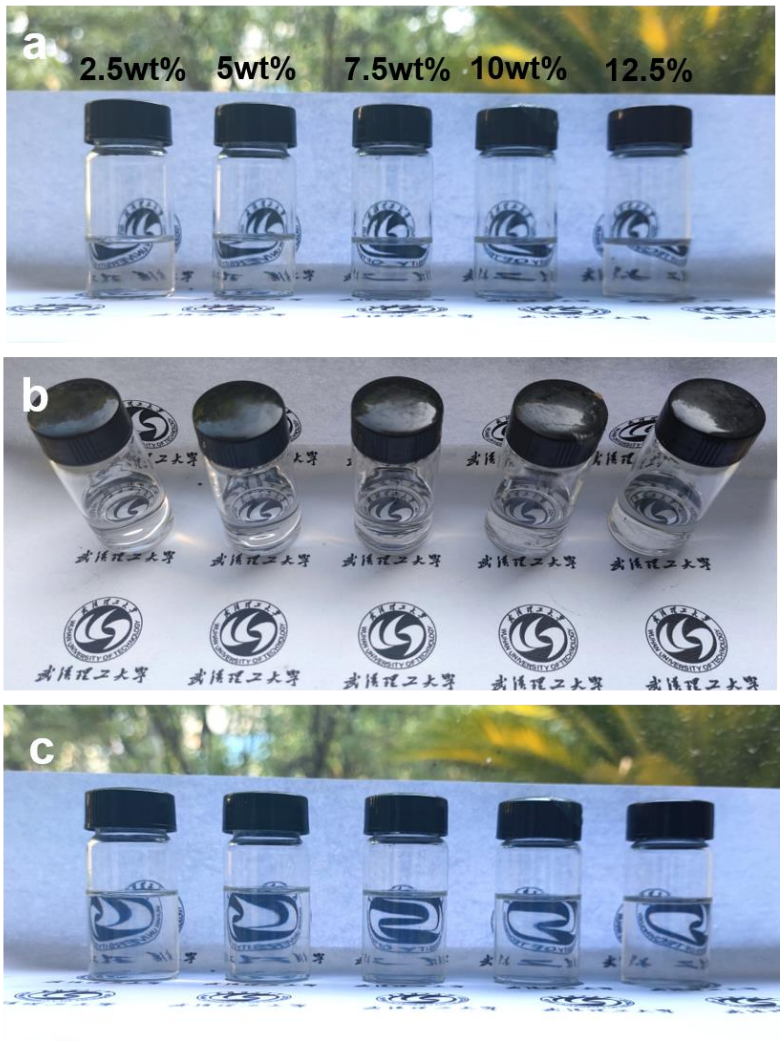

Figure S2. Images of a,b) cluster chain mixtures and c) cluster chain based solid electrolyte mixtures. Mass fraction of cluster chain is from 2.5 wt% to 12.5 wt%, respectively.

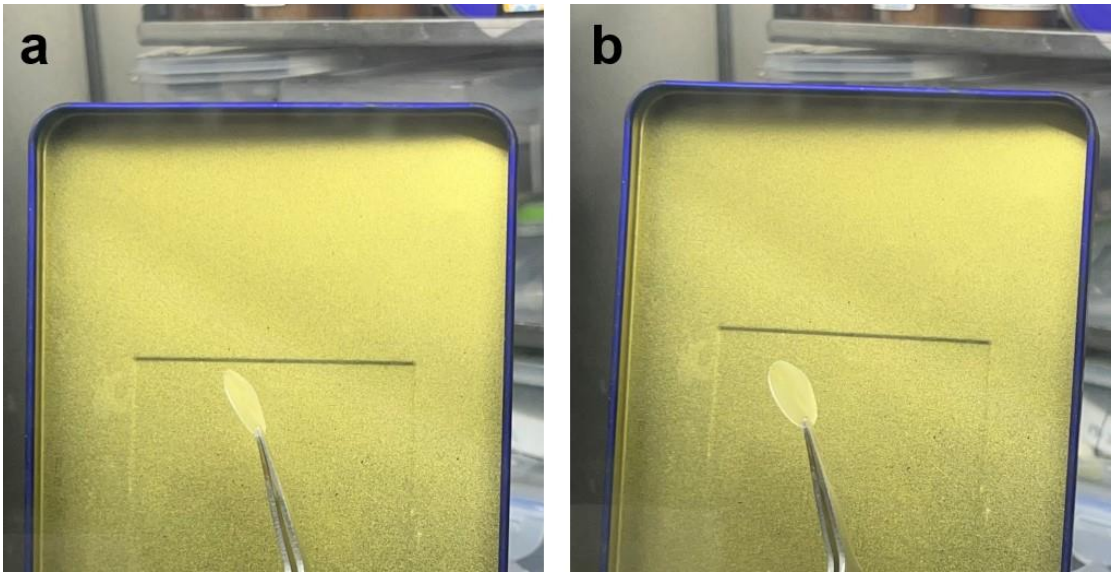

Figure S3. The optical photos of the CPCSE membrane.

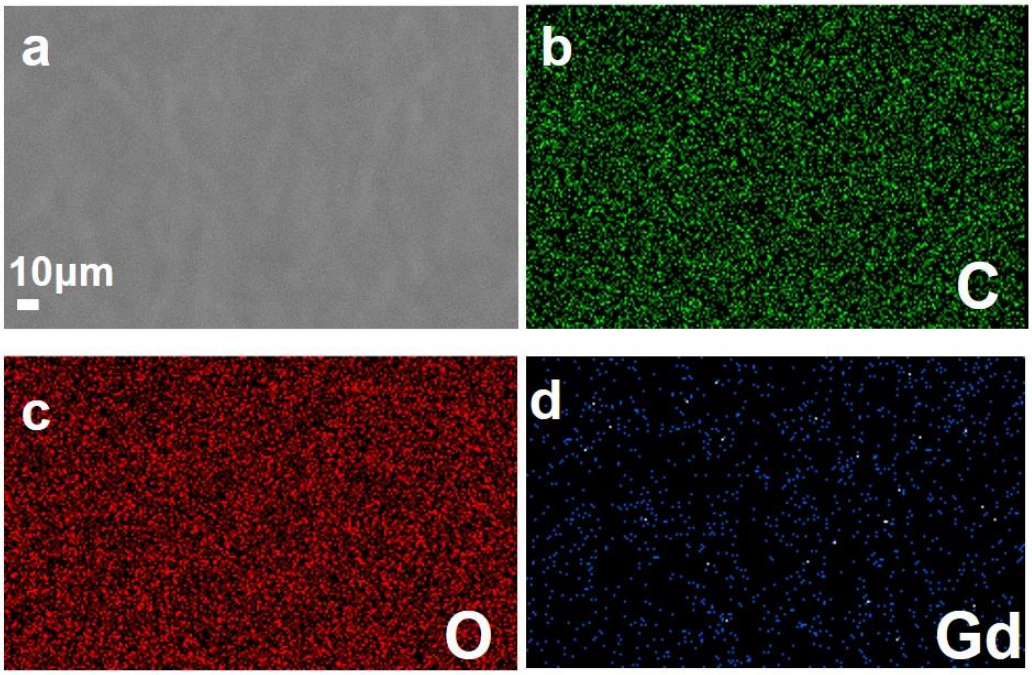

Figure S4. a) SEM image of CPCSE and EDS mapping images of b-d) C, O, Gd element.

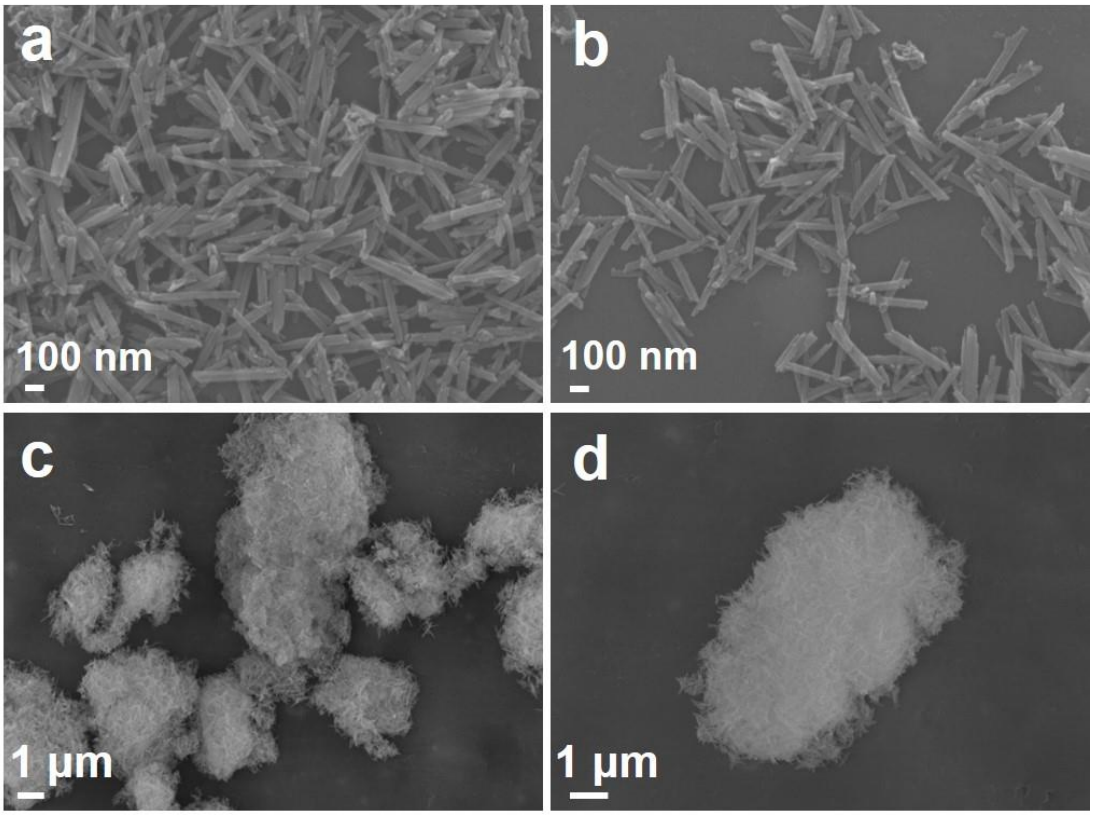

Figure S5. SEM images of common nanowires.

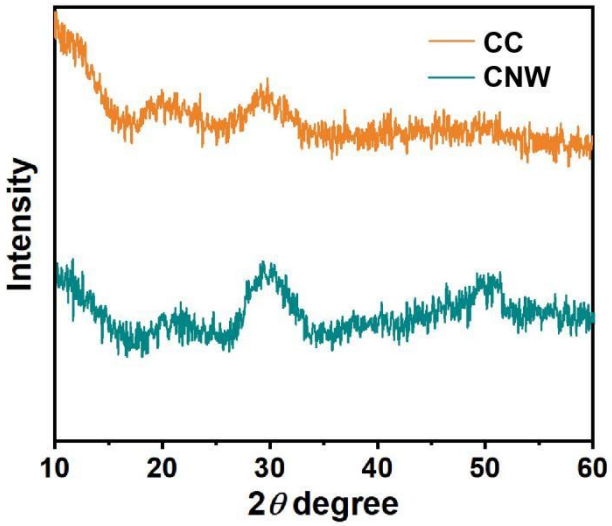

Figure S6. XRD pattern of cluster chains and common nanowires.

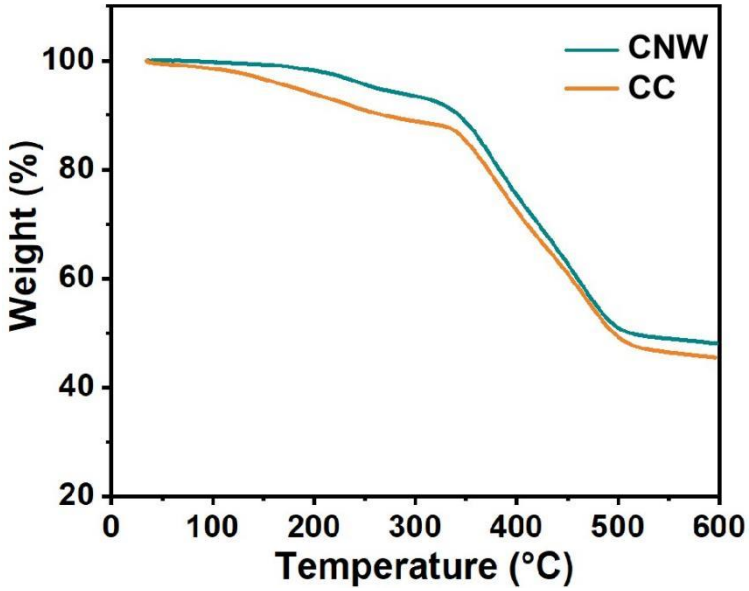

Figure S7. Thermogravimetric analysis of cluster chains and common nanowires.

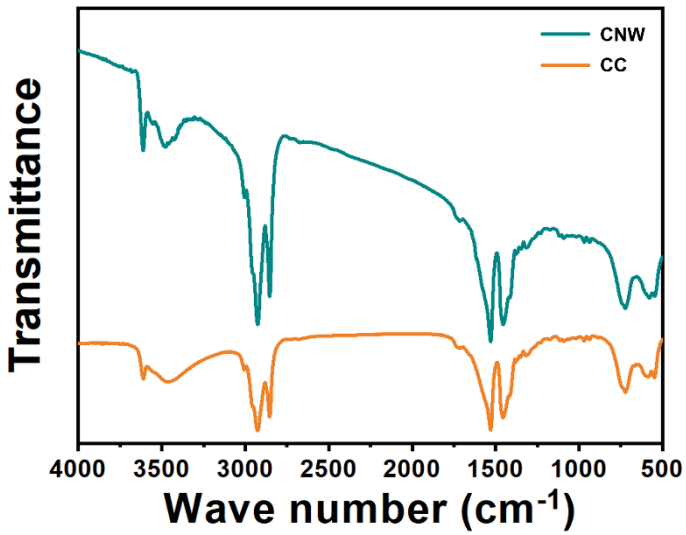

Figure S8. The Fourier transform infrared spectroscopy (FT-IR) spectra of cluster chains and common nanowires.

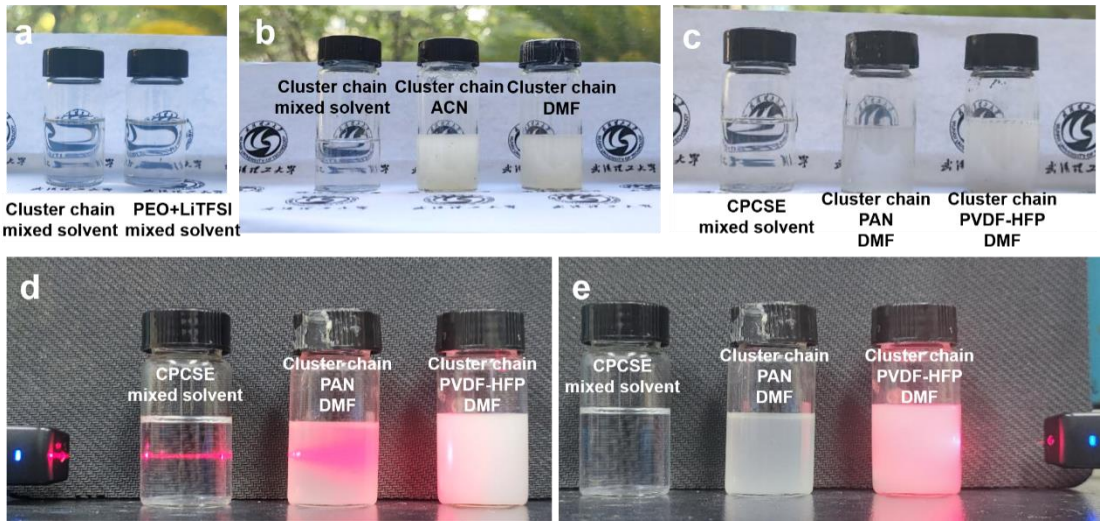

Figure S9. Optical photographs of a) Cluster chain and PEO+LiTFSI in mixed solvent. b) Cluster chain in mixed solvent, ACN, and DMF. c) SSE mixtures of CPCSE in mixed solvent, cluster chain+PAN+DMF, cluster chain+PVDF-HFP+DMF. d,e) Optical photographs of Tyndall effect in SSE mixtures.

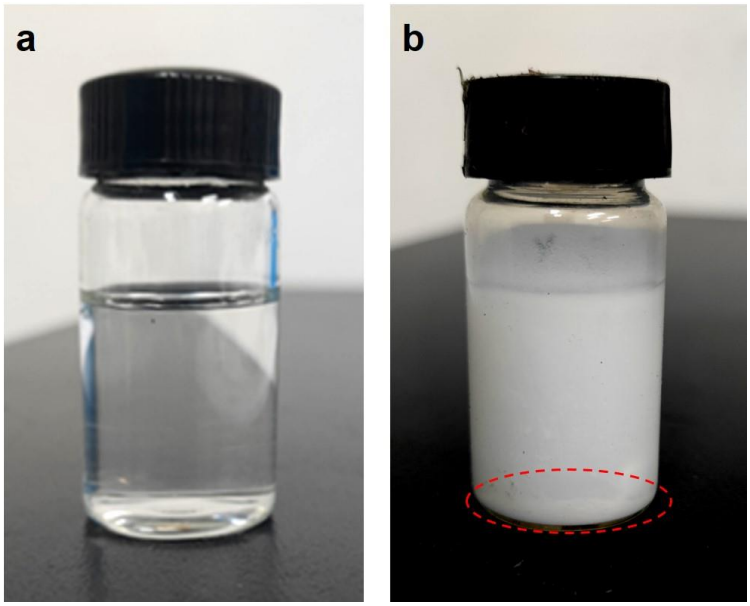

Figure S10. The optical photos of the a) CPCSE and b) CNCSE mixture after 2 weeks standing

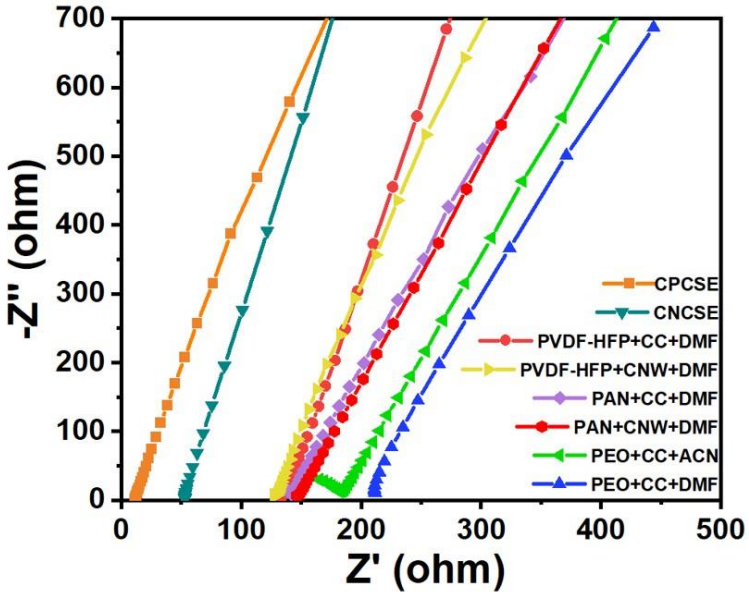

Figure S11. EIS curves of different solid-state electrolytes at room temperature.

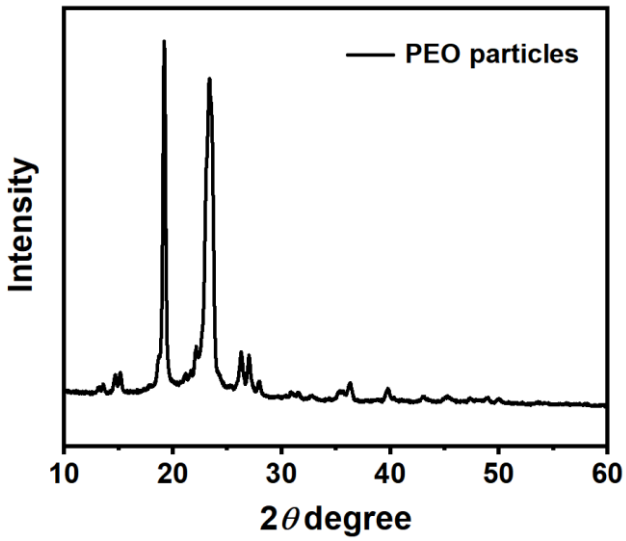

Figure S12. XRD pattern of PEO powders.

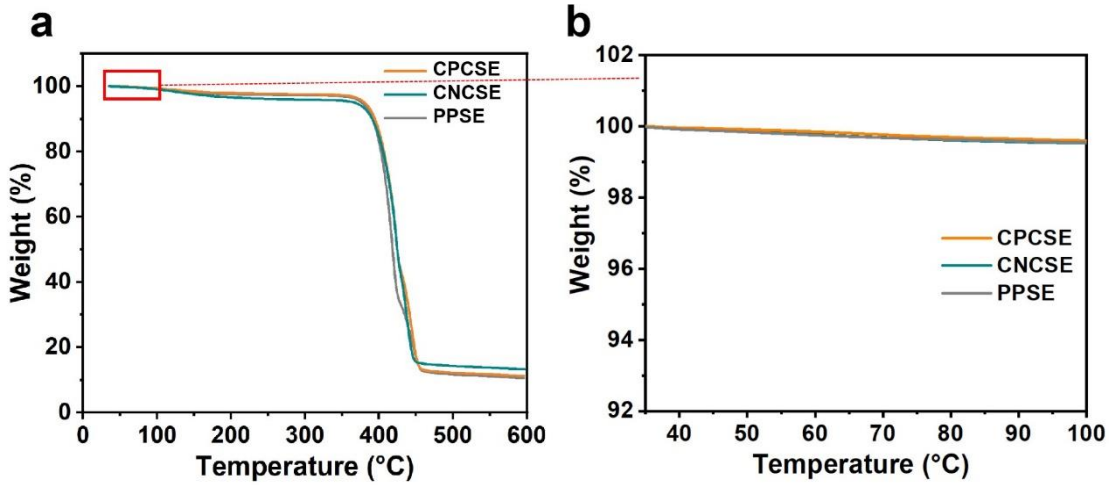

Figure S13. a) Thermogravimetric curves of CPCSE, CNCSE, and PPSE membranes from 35 °C to 600 °C. b) The enlarged thermogravimetric curves from 35 °C to 100 °C.

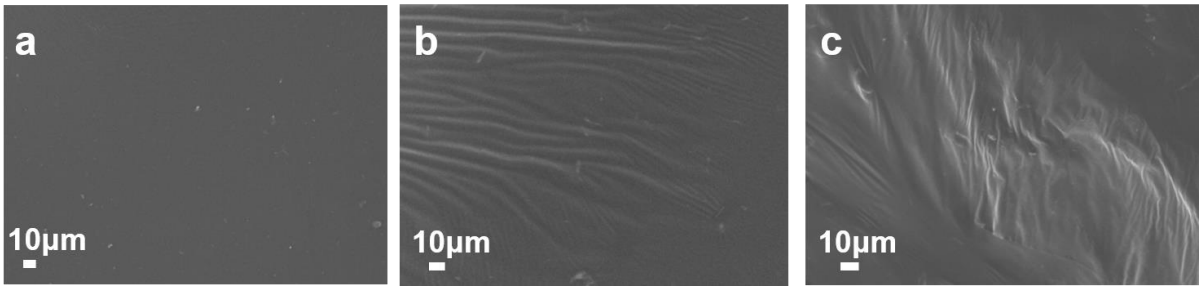

Figure S14. SEM images of a) CPCSE, b) CNCSE and (c) PPSE films.

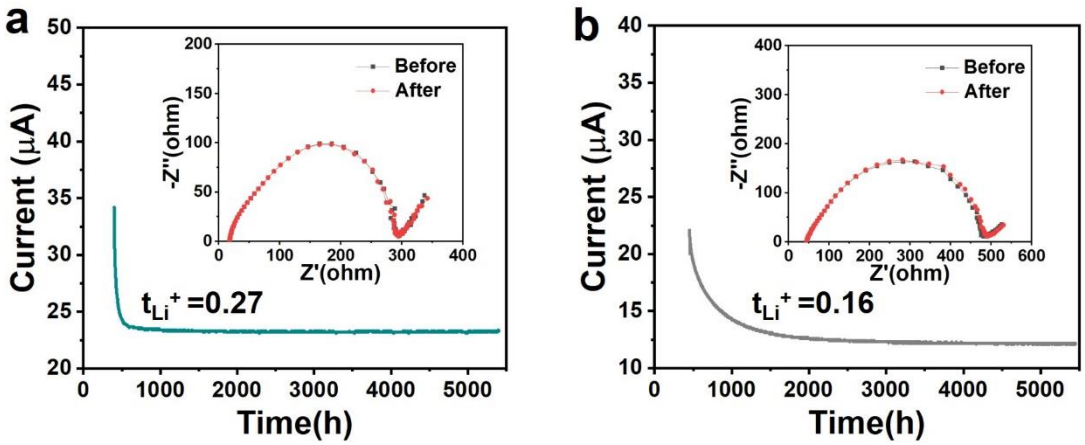

Figure S15. Current-time curves of Li symmetric cell, inserting is the corresponding EIS curves before and after polarization. a) CNCSE, b) PPSE.

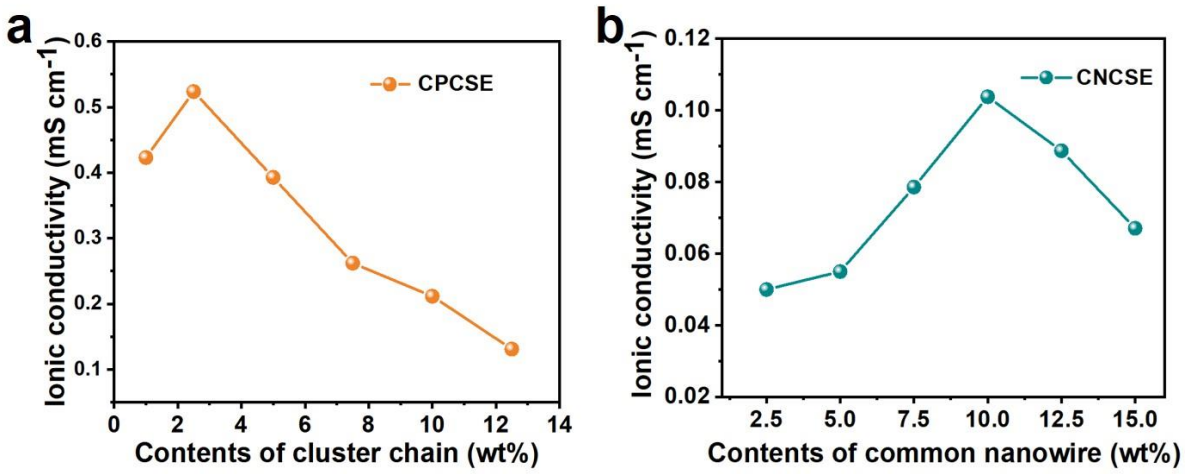

Figure S16. Distribution plots of ionic conductivity with different filler mass. a) CPCSE, b) CNCSE.

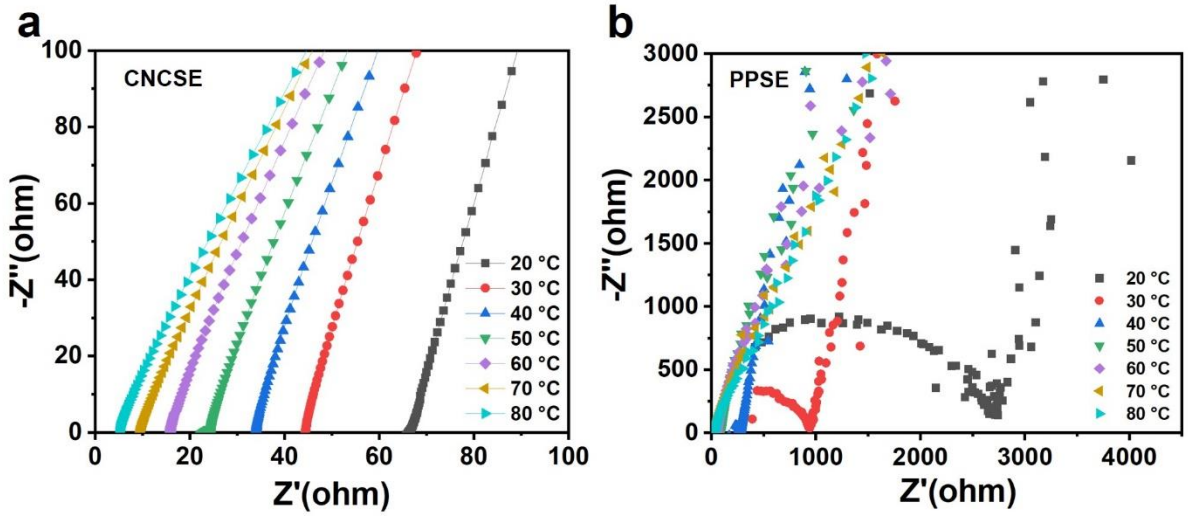

Figure S17. EIS curves of a) CNCSE and b) PPSE at different temperatures.

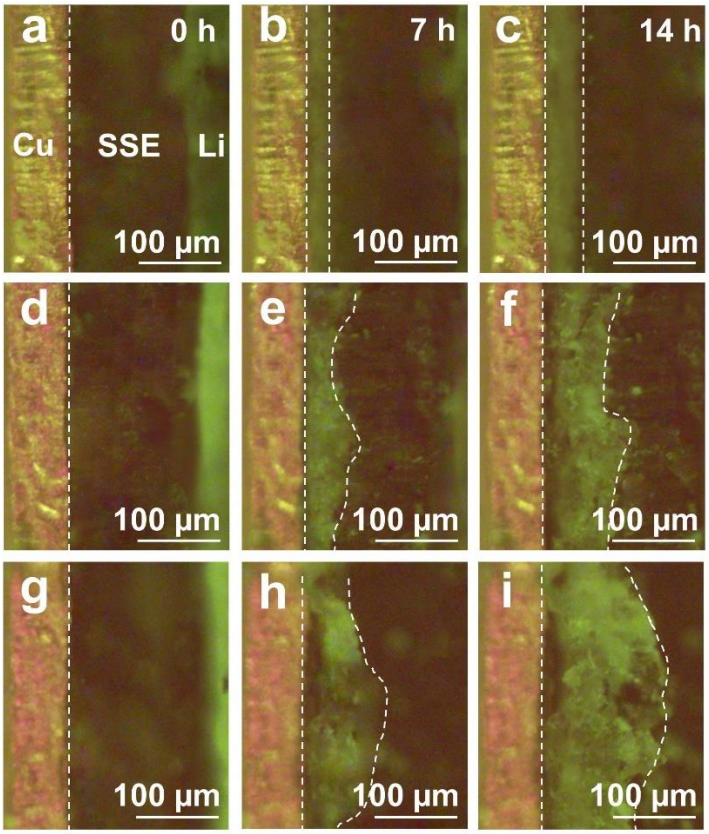

Figure S18. Lithium deposition morphologies of the Cu/CSE/Li battery a-c) CPCSE, d-f) CNCSE, g-i) PPSE after 0 h, 7 h, 14 h cycling at a current density of 0.15 mA cm^{-2} and room temperature.

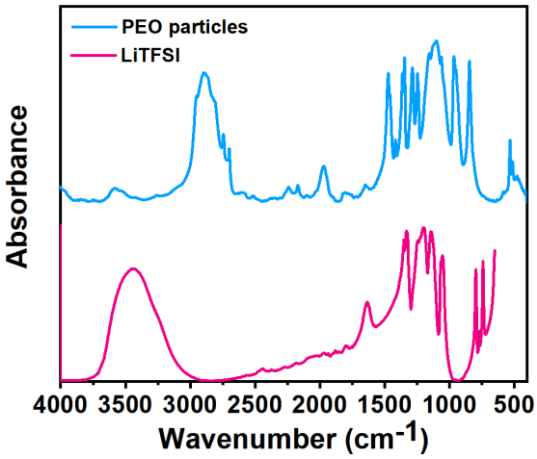

Figure S19. FT-IR spectra of PEO particles and LiTFSI.

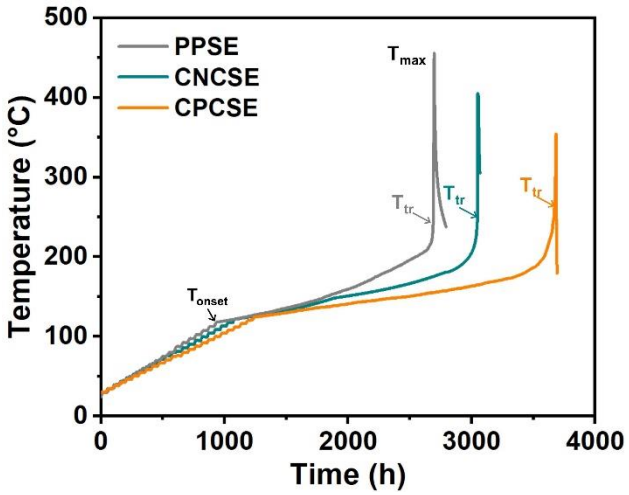

Figure S20. Temperature-time curves of ARC tests for NCM/Li pouch cells.

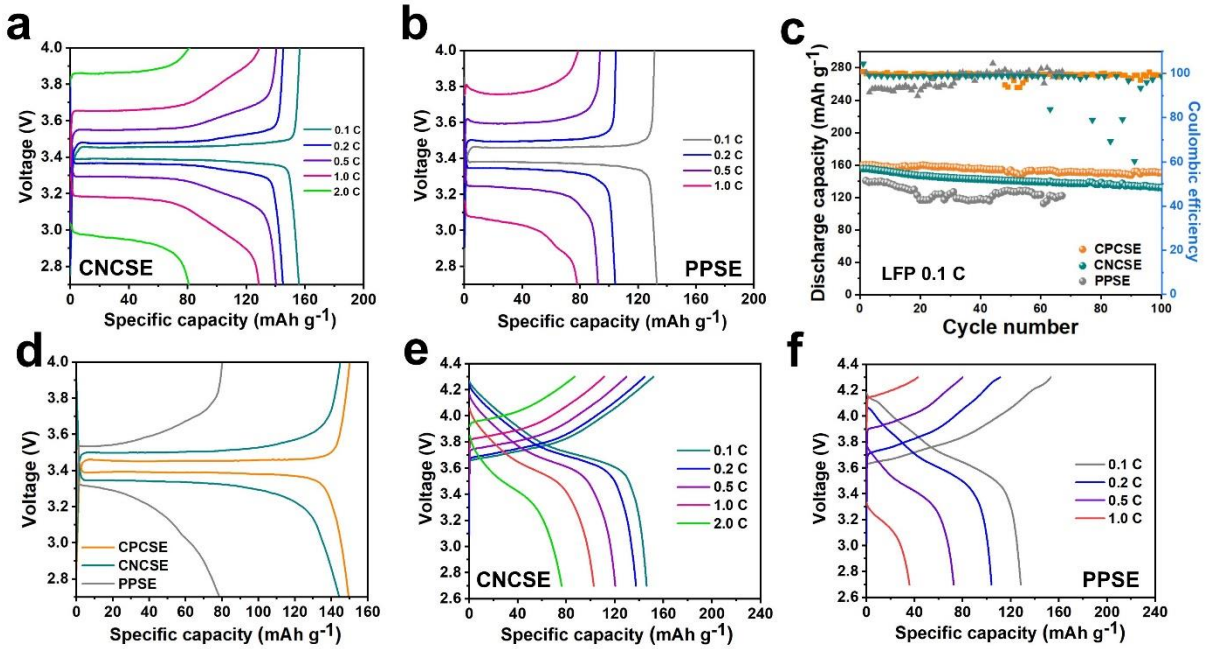

Figure S21. Voltage-capacity profiles of LFP/Li solid-state full cells with a) CNCSE and b) PPSE under different current densities. c) Cycling performance of the LFP/Li solid-state full cells at 0.1 C. d) The 100th cycle voltage-capacity profiles of LFP/Li solid-state full cells at 0.5 C. Voltage-capacity profiles of NCM811/Li solid-state full cells with e) CNCSE and f) PPSE.

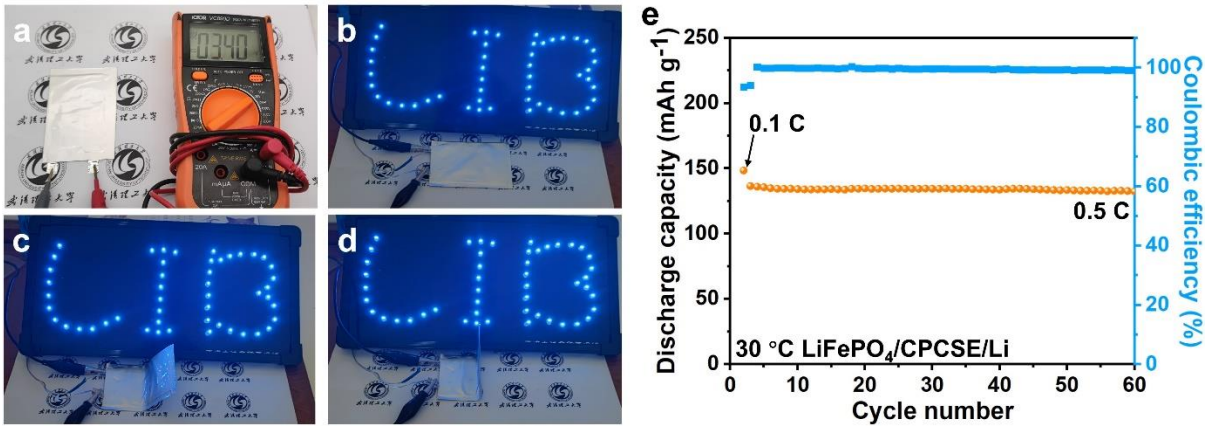

Figure S22. a) Optical photographs of the open circuit voltage test of the flexible LFP/CPCSE/Li cell. b-d) Optical photographs of LFP/CPCSE/Li pouch cell lighting up the LED in series under flat and different folding conditions. e) Cycling performance of the LFP/CPCSE/Li pouch cell at current density of 0.5 C and 30 °C.

Table S1. Cycling performance of NCM/Li solid-state batteries.

	Solid-state electrolyte	Cathode material	Current density	Capacity retention	Reference
Our work	Inorganic cluster chains/PEO	NCM 811	0.5 C	142.8 mA h/g after 250 cycles 93.7 %	
1	$Li_{0.33}La_{0.56}TiO_{3-x}$ nanofiber/PVDF-b-PTFE	NCM 532	0.2 C	120 mA h/g after 200 cycles	Adv. Mater.[1]
2	Li_6PS_5Cl	NCM 83	0.1 C	86 % after 100 cycles	Adv. Energy Mater.[2]
3	PEO/LiTFSI/GO-g-PSSLi	NCM 811	0.5 C	83 % after 100 cycles	Adv. Mater.[3]
4	PEO /porous ceramic scaffold	NCM 811	0.35 mA/cm^2	177 mAh/g after 100 cycles 78%	Adv. Mater.[4]
5	PEO/2D-MOF	NCM 523	0.2 C	138.1 mAh/g after 100 cycles 71%	Adv. Mater.[5]
6	Superconcentrated ionogel-in- LLZO	NCM 523	1 C	139 mA h/g after 200 cycles 72.7 %	Adv. Mater.[6]
7	Plastic crystal-embedded elastomer electrolytes	NCM 83	0.2 C	188 mA h/g after 100 cycles 92.4 %	Adv. Mater.[7]
8	$Li_{0.33}La_{0.56}TiO_{3-x}$ nanofiber/PVDF/PTFE	NCM 523	0.2 C	120 mA h/g after 200 cycles.	Adv. Mater.[8]
9	Li_2S/PEO	NCM 811	0.2 C	91.2 % after 150 cycles	Adv. Mater.[9]
10	PAN/LAGP/PEGDA	NCM 622	0.5 C	81.5% after 270 cycles	Adv. Mater.[10]
11	Dual-polymer electrolyte	NCM 622	0.2 mA/cm^2	80.9 % after 100 cycles	Adv. Energy Mater.[11]
12	$Li_{10}SnP_2S_{12}$	NCM 811	0.1 C	64.5 % after 100 cycles	Adv. Energy Mater.[12]

Table S2. Key performance parameters of PEO-based composite solid electrolytes with different inorganic fillers.

SSEs	Ionic conductivity (S cm^{-1})	Li-Li cycling	Cycling performance (mAh g^{-1})	Rate performance (mAh g^{-1})	Li^+ transference number	Ref.
Our work	**5.2×10^{-4} (room temperature)**	**1000 h, 40mV (0.1 mA cm^{-2}, 60 ℃)**	**130 (1000th, 0.5 C, 88.1%, 60 ℃) 115 (700th, 1 C, 81.2%, 60 ℃)**	**120 (2 C, 60 ℃)**	**0.62**	**/**
Ca-doped CeO_2 ($Ca–CeO_2$) nanotube	1.3×10^{-4} (60 ℃)	1000 h, 80 mV (0.1 mA cm^{-2}, 60 ℃)	93 (200th, 1 C, 60 ℃)	100 (2 C, 60 ℃)	0.453	Adv. Energy Mater.[13]
$Mg_2B_2O_5$ nanowire	1.53×10^{-4} (40 ℃)	650 h, 55 mV (0.1 mA cm^{-2}, 50 ℃)	120 (230th, 1 C, 50 ℃)	72 (2 C, 50 ℃)	/	Nano Lett.[14]
Li_2S_6	1.7×10^{-4} (40 ℃)	400 h, 250 mV (0.2 mA cm^{-2}, 40 ℃)	108.7 (100th, 0.1 mA cm^{-2}, 81%, 40 ℃)	86.5 (0.3 mA cm^{-2}, 40 ℃)	0.23	Angew. Chem. Int. Ed.[15]
Li_2S	1.3×10^{-5} (30 ℃)	1800 h, 50 mV (0.1 mA cm^{-2}, 50 ℃)	140 (1000th, 0.5 C, 85%, 50 ℃)	83 (2 C, 50 ℃)	0.4	Adv. Mater.[16]
$Gd_{0.1}Ce_{0.9}O_{1.95}$	1.9×10^{-4} (30 ℃)	800 h, 100 mV (0.1 mA cm^{-2}, 35 ℃)	100 (100th, 0.1 mA cm^{-2}, 99%, 35 ℃)	108 (0.15 mA cm^{-2}, 35 ℃)	0.26,	Angew. Chem. Int. Ed.[17]
Nb/Al co-doped LLZO+SN	3.09×10^{-4} (room temperature)	400 h, 100 mV (0.05 mA cm^{-2}, 60 ℃)	129.9 (200th, 0.2 C, 90%, 45 ℃)	130 (2 C, 45 ℃)	0.75	Adv. Funct. Mater.[18]

I_2	7.17×10^{-5} (50 °C)	600 h, 63 mV (0.1 mAh cm^{-2}, 50 °C)	150 (300^{th}, 0.5 C, 96.5%, 50 °C)	/	/	Adv. Funct. Mater.[19]
MoO_3 nanobelt	1.16×10^{-3} (60 ℃)	1000 h, 90 mV (0.2 mAh cm^{-2}, 60 ℃)	140 (350^{th}, 0.5 C, 60℃)	120 (2 C, 60 ℃)	0.57	Adv. Funct. Mater.[20]
LLZO nanoparticle	1.05×10^{-4} (50 °C)	1000 h, 90 mV (0.1 mA cm^{-2}, 50 °C)	147.6 (180^{th}, 0.2 C, 99.2%, 50 ℃)	130.8 (2 C, 60 ℃)	0.45	Nano Lett.[21]
$Li_{3/8}Sr_{7/16}Ta_{3/4}Zr_{1/4}O_3$	5.4×10^{-5} (25 °C)	700 h, 57 mV (0.1 mA cm^{-2}, 45 °C)	150 (350^{th}, 0.15 mA cm^{-2}, 99.5%, 45 °C)	128 (0.2 mA cm^{-2}, 45 ℃)	0.43	Proc. Natl. Acad. Sci. U. S. A.[22]

Reference

[1] S. Liu, Y. Zhao, X. Li, J. Yu, J. Yan, B. Ding, *Adv. Mater.* **2021**, 33, 2008084.

[2] B. Shi, Y. Yusim, S. Sen, T. Demuth, R. Ruess, K. Volz, A. Henss, F. H. Richter, *Adv. Energy Mater.* **2023**, 13, 2300310.

[3] Q. Liu, R. Liu, Y. Cui, M. Zhou, J. Zeng, B. Zheng, S. Liu, Y. Zhu, D. Wu, *Adv. Mater.* **2022**, 34, 2108437.

[4] F. He, We. Tang, X. Zhang, L. Deng, J. Luo, *Adv. Mater.* **2021**, 33, 2105329.

[5] L. Xu, X. Xiao, H. Tu, F. Zhu, J. Wang, H. Liu, W. Huang, W. Deng, H. Hou, T. Liu, X. Ji, K. Amine, G. Zou, *Adv. Mater.* **2023**, DOI: 10.1002/adma.202303193.

[6] Y. Zhai, W. Hou, M. Tao, Z. Wang, Z. Chen, Z. Zeng, X. Liang, P. Paoprasert, Y. Yang, N. Hu, S. Song, *Adv. Mater.* **2022**, 34, 2205560.

[7] J. Han, M. J. Lee, K. Lee, Y. J. Lee, S. H. Kwon, J. H. Min, E. Lee, W. Lee, S. W. Lee, B. J. Kim, *Adv. Mater.* **2023**, 35, 2205194.

[8] S. Liu, Y. Zhao, X. Li, J. Yu, J. Yan, B. Ding, *Adv. Mater.* **2021**, 33, 2008084.

[9] O. Sheng, J. Zheng, Z. Ju, C. Jin, Y. Wang, M. Chen, J. Nai, T. Liu, W. Zhang, Y. Liu, X. Tao, *Adv. Mater.* **2020**, 32, 2000223.

[10] H. Duan, M. Fan, W.-P. Chen, J.-Y. Li, P.-F. Wang, W.-P. Wang, J.-L. Shi, Y.-X. Yin, L.-J. Wan, Y.-G. Guo, *Adv. Mater.* **2019**, 31, 1807789.

[11] X. Pan, H. Sun, Z. Wang, H. Huang, Q. Chang, J. Li, J. Gao, S. Wang, H. Xu, Y. Li, W. Zhou, *Adv. Energy Mater.* **2020**, 10, 2002416.

[12] X. Liu, B. Zheng, J. Zhao, W. Zhao, Z. Liang, Y. Su, C. Xie, K. Zhou, Y. Xiang, J. Zhu, H. Wang, G. Zhong, Z. Gong, J. Huang, Y. Yang, *Adv. Energy Mater.* **2021**, 11, 2003583.

[13] H. Chen, D. Adekoya, L. Hencz, J. Ma, S. Chen, C. Yan, H. Zhao, G. Cui, S. Zhang, *Adv. Energy Mater.* **2020**, 10, 2000049.

[14] O. Sheng, C. Jin, J. Luo, H. Yuan, H. Huang, Y. Gan, J. Zhang, Y. Xia, C. Liang, W. Zhang, X. Tao, *Nano Lett.* **2018**, 18, 3104.

[15] R. Fang, B. Xu, N. S. Grundish, Y. Xia, Y. Li, C. Lu, Y. Liu, N. Wu, J. B. Goodenough, *Angew. Chem. Int. Ed.* **2021**, 60, 17701.

[16] O. Sheng, J. Zheng, Z. Ju, C. Jin, Y. Wang, M. Chen, J. Nai, T. Liu, W. Zhang, Y. Liu, X. Tao, *Adv. Mater.* **2020**, 32, 2000223.

[17] N. Wu, P.-H. Chien, Y. Qian, Y. Li, H. Xu, N. S. Grundish, B. Xu, H. Jin, Y. Hu, G. Yu, J. B. Goodenough, *Angew. Chem. Int. Ed.* **2020**, 59, 4131.

[18] H. L. Nguyen, V. T. Luu, M. C. Nguyen, S. H. Kim, Q. H. Nguyen, N. I. Nungu, Y.-S. Jun, W. Ahn, *Adv. Funct. Mater.* **2022**, 32, 2207874.

[19] O. Sheng, H. Hu, T. Liu, Z. Ju, G. Lu, Y. Liu, J. Nai, Y. Wang, W. Zhang, X. Tao, *Adv. Funct. Mater.* **2022**, 32, 2111026.

[20] X. Wang, S. Huang, K. Guo, Y. Min, Q. Xu, *Adv. Funct. Mater.* **2022**, 32, 2206976

[21] M. Zhang, P. Pan, Z. Cheng, J. Mao, L. Jiang, C. Ni, S. Park, K. Deng, Y. Hu, K. K. Fu, *Nano Lett.* **2021**, 21, 7070.

[22] H. Xu, P.-H. Chien, J. Shi, Y. Li, N. Wu, Y. Liu, Y.-Y. Hu, J. B. Goodenough, *Proc. Natl. Acad. Sci. U. S. A.* **2019**, 116, 18815.